Rapid ozone depletion after humidification of the stratosphere by the Hunga Tonga Eruption

Stephanie Evan, Jerome Brioude, Karen Rosenlof, Ru-Shan Gao, Robert Portmann, Yunqian Zhu, Rainer Volkamer, Christopher Lee, Jean-Marc Metzger, Kevin Lamy, et al.

Title: Rapid ozone loss following humidification of the stratosphere by the Hunga Tonga Eruption

Authors: Stephanie Evan[1*], Jerome Brioude[1], Karen H. Rosenlof[2], Ru-Shan Gao[2], Robert W. Portmann[2], Rainer Volkamer[3], Christopher F. Lee[3], Jean-Marc Metzger[4], Kevin Lamy[1], Paul Walter[5], Sergio L. Alvarez[6], James H. Flynn[6], Elizabeth Asher[2,7], Michael Todt[2,7], Sean M. Davis[2], Troy Thornberry[2], Holger Vömel[8], Frank G. Wienhold[9], Ryan M. Stauffer[10], Luis Millán[11], Michelle L. Santee[11], Lucien Froidevaux[11], William G. Read[11]

Affiliations :

[1]Laboratoire de l'Atmosphère et des Cyclones (LACy, UMR8105, CNRS, Université de La Réunion, Météo-France), Saint-Denis, France.
[2]NOAA Chemical Sciences Laboratory, Boulder, United States.
[3]Department of Chemistry and Cooperative Institute for Research in Environmental Sciences, University of Colorado, Boulder, United States.
[4]Observatoire des Sciences de l'Univers de la Réunion, UAR 3365 (CNRS, Université de la Réunion, Météo-France), Saint-Denis, France.
[5]St. Edward's University, Austin, United States.
[6] University of Houston, Houston, United States.
[7]Cooperative Institute for Research in Environmental Sciences, University of Colorado Boulder, United States?
[8]National Center for Atmospheric Research, Boulder, United States.
[9]Swiss Federal Institute of Technology (ETH), Zurich, Switzerland.
[10]NASA Goddard Space Flight Center, Atmospheric Chemistry and Dynamics Lab, Greenbelt, United States.
[11]Jet Propulsion Laboratory, California Institute of Technology, Pasadena, United States.

*Corresponding author. Email: stephanie.evan@univ-reunion.fr

Abstract:
The massive January 2022 Hunga Tonga–Hunga Ha'apai eruption produced major perturbations in atmospheric composition, increasing the stratospheric water burden by 10%. Fresh stratospheric volcanic plume measurements are rare, but unique circumstances allowed in-situ tropical profiles of H_2O, aerosols, and O_3 at the Maïdo Observatory within a week of the eruption. Analysis including remote sensing observations of O_3, HCl, ClO and NO_2 radicals shows chemical O_3 loss (-0.5 ppmv between 25-30 km in a week) in the volcanic plume under unusually warm temperatures (T ~ 220 K at 28 km). This rapid loss indicates that heterogeneous chlorine activation is efficient on humidified volcanic aerosols. Although a rare occurrence, better understanding of these processes provide insight on ozone perturbations possible in a world with changing climate.

One-Sentence Summary: The 2022 Hunga Tonga–Hunga Ha'apai eruption majorly perturbed tropical stratospheric water and aerosols producing rapid ozone loss in the plume.

Main Text:

Large explosive volcanic eruptions can impact the climate by injecting gases (sulfur dioxide (SO_2), water vapor (H_2O), carbon dioxide (CO_2), and halogen compounds such as hydrochloric acid (HCl) into the stratosphere. Typically, sulfate aerosols form from SO_2 on a timescale of weeks; these aerosols cool the surface by reflecting some incoming solar radiation and warm the stratosphere via absorption of longwave radiation. Sulfate aerosol heating can alter stratospheric transport affecting the distribution of stratospheric species (*1*). The increase in the aerosol burden also enhances aerosol surface area density, increasing the chances for heterogeneous chemical reactions that play a role in stratospheric ozone chemistry.

Previous volcanic eruptions had a noticeable impact on stratospheric ozone (e.g., El Chichón in 1982 (*2*, *3*), Mt. Pinatubo in 1991 (*4*, *5*). Following the eruption of Mt. Pinatubo, the total ozone column was reduced by ~6% in north polar and midlatitude regions (*6*). The ozone was destroyed by chemical reactions on volcanic aerosols transported to high latitudes, which provided additional reactive surface area for the same heterogeneous chemical reactions that cause polar ozone loss each year. In the tropics, a 6% decrease in total ozone was observed in satellite and ozonesonde data (*7*). It was confined between 24 and 28 km in altitude and started a month after the eruption, consistent with the time needed for SO_2 to be converted to sulfate aerosols (*8*).

To quantify the ozone loss on volcanic aerosols, we need information on aerosol size/concentration, trace gases (e.g., ozone, chlorinated species) and meteorological conditions (temperature, humidity) following the eruptions. Major eruptions that cause large perturbations to the aerosol loading and ozone chemistry of the stratosphere occur sporadically, so the opportunity to make measurements in these plumes is rare.

The Hunga Tonga–Hunga Ha‘apai submarine volcano (hereafter HT) in the South Pacific (20.55°S, 175.38°W) was the largest volcanic eruption in the past 30 years. Its massive eruption on 15 January 2022 sent material as high as 50-55 km, the greatest height ever reported for a volcanic plume (*9*, *10*). Satellite measurements indicated that the HT volcano injected into the stratosphere a relatively small amount of SO_2 (0.4 Tg (*10*) as compared to an amount of 10-20 Tg from Mt.. Pinatubo (*11*, *12*), but a massive amount of H_2O (~150 Tg, or 10% of the stratospheric burden (*10*) unlike past eruptions. The large amount of H_2O injected was also confirmed by radiosonde in situ measurements (*13*).

Less than a week after the eruption, a rapid response balloon campaign took place at the Maïdo Observatory (MO) in Réunion Island, 21°S, 55°E) (*14*). Due to zonal easterly winds in the stratosphere (20-50 km), Réunion Island was ideally located downwind of the plume. From 20 to 24 January 2022, multiple meteorological balloons carrying aerosol, H_2O, SO_2 and ozone instruments were launched each night to provide key measurements of the volcanic plume composition (see Methods). A field campaign resulting in volcanic plume measurements in the stratosphere by in situ instruments has never occurred this quickly post-eruption. In comparison, a rapid response balloon campaign was deployed to Hawaii within 15 days of the 2018 Kilauea eruption (*15*). In this paper, we present unique observations that corroborate the occurrence of fast chemical ozone loss inside the volcanic plume in the week following the eruption. The extremely high water vapor values accelerated the oxidation of SO_2 to sulfate aerosols, with

much of the conversion in the densest parts of the plume occurring within a few days after the eruption (*16*), facilitating heterogeneous chemical ozone loss. Additionally, as noted by Anderson et al. (2012) (*17*), high stratospheric water vapor can change the catalytic chlorine free radical chemistry by shifting total available inorganic chlorine ClO, potentially increasing ozone loss. Both rapid aerosol conversion and additional ozone loss appeared very rapidly for the HT eruption. The high vertical resolution in situ measurements were critical for seeing this loss which is not easily apparent in the satellite ozone observations that smear features in the vertical.

Results*:*

Fig. 1 shows balloon-borne measurements of ozone and H_2O profiles at MO for the period 20-24 January 2022. It took 6 days for the volcanic plume to reach Réunion at ~30 km altitude. Balloon measurements five days after the eruption indicate typical stratospheric background values of H_2O (4.5 ppmv) and a peak in ozone partial pressure of 15 mPa at 25 km. At Reunion, the highest H_2O mixing ratio of 356 ppmv at 27 km was reported on 22 January, 21 UTC. Larger values of near 1000 ppmv were indicated in radiosonde measurements closer to the eruption by Vömel et al. (2022)(*13*). The observed progression of descending altitude with time in the peak of the H_2O plume in Fig. 1 can be explained by the vertical sheer in easterly zonal winds that linearly decreased from 30 m s^{-1} at 30 km to 20 m s^{-1} at 20 km; causing the plume to travel ~18° in longitude per day (*10*, *13*).

The largest ozone decrease was observed on 21 and 22 January at 25-29 km. The decrease amounts to a loss of 10-45% of the 1998-present ozone climatology (see Methods in Supplemental Material). The presence of SO_2 inside the volcanic plume could affect the performance of ECC ozonesondes by decreasing the sensor signal, resulting in artificially low ozone measurements. During the experiment, SO_2 instruments (*18*) were launched in tandem with ECC ozonesondes on three flights (see Methods). Overall, SO_2 data indicate that SO_2 interference accounts for only 3-4% of the ozone decrease observed above 25 km the week after the eruption (see Methods).

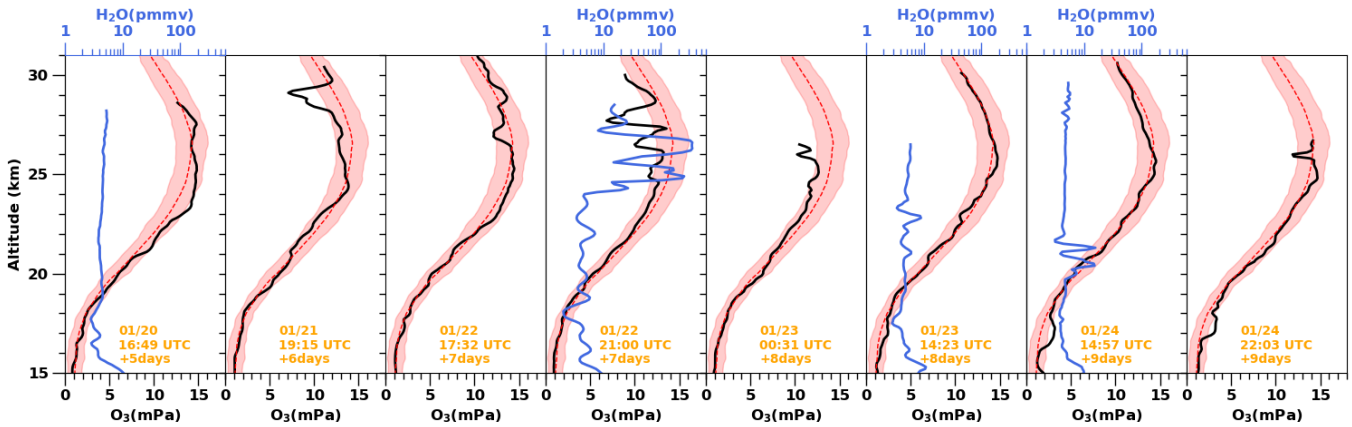

Fig. 1. Soundings of ozone and water vapor a week after the eruption. Profiles of ozone partial pressure (black) and water vapor mixing ratio (blue) measured at Maïdo Observatory on Réunion Island over 20-24 January 2022. SHADOZ climatological ozone partial pressure for January for Réunion Island is indicated by the red dashed line. The red shaded area shows values of 2 standard deviations above and below the mean.

Satellite measurements of stratospheric gas profiles from the Aura Microwave Limb Sounder (MLS), in operation since 2004 (*19*) were also used to diagnose possible mechanisms of ozone decrease following the eruption. As MLS measures microwave thermal emission from the Earth's limb, its retrievals are largely unaffected by the presence of volcanic aerosols that strongly impair visible, ultraviolet, and infrared measurements. MLS observed the massive H_2O perturbation as well as anomalous values of several trace gases injected into the stratosphere by HT, such as SO_2 and HCl (*10*). Large H_2O values more than 100 standard deviations (σ) above background levels were observed in the week following the eruption between 20 and 30 km, with a maximum value as high as 350 ppmv at 30 km on 16 January. In Fig. 2, MLS measurements of ozone, HCl and ClO radicals inside the volcanic plume are identified by selecting data points which have water vapor mixing ratios above 10 ppmv between 100 and 10 hPa (see Methods). Then for each data point, the climatological January 2005-2021 average profile is computed by using MLS profiles in a 5°x5° box region around the point (see Methods). MLS ozone mixing ratios inside the volcanic plume decreased at 18-21 hPa (~27-28 km) in the week following the HT eruption, from an average value of 6.3 ppmv on 16 January to a minimum value of 4.6 ppmv on 20 January (near 18°S, 88°E) at 21 hPa, 27% below climatological values.

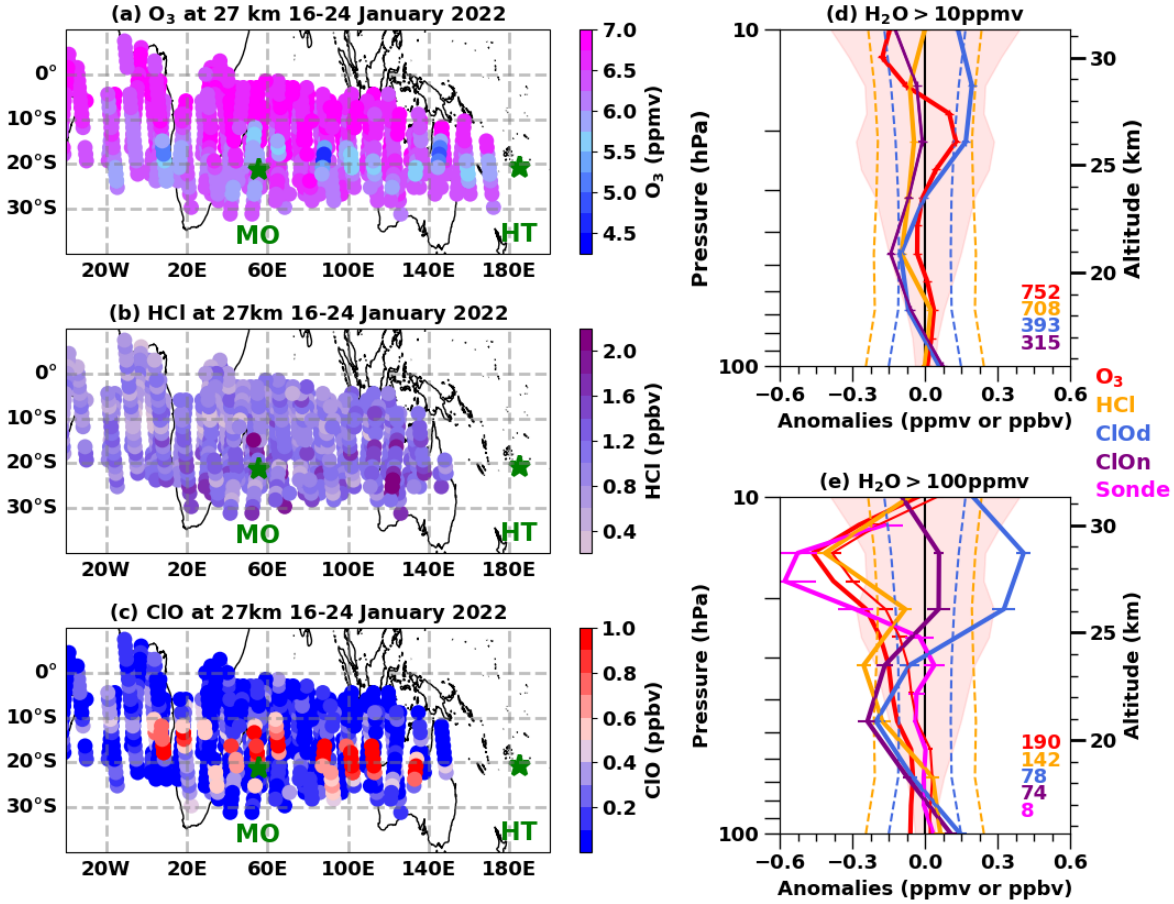

Fig. 2: MLS satellite measurements inside the volcanic plume. Maps of MLS (a) ozone, (b) HCl and (c) ClO at 27 km for the period 16-24 January 2022. The locations of the Hunga Tonga volcano (HT) and the Maïdo Observatory (MO) are indicated by green stars. Colored circles correspond to individual satellite profiles. MLS anomaly profiles (see Methods) of (d) ozone (ppmv, red), HCl (ppbv, orange) and ClO (ppbv, blue and purple) inside the volcanic plume averaged over the period 16-24 January.

Anomalies are computed for MLS measurements inside the plume using a water vapor threshold of 10 ppmv. (e) Same as (d) for but H_2O mixing ratios exceeding 100 ppmv. The red shaded area in panels (d) and (e) indicates the ± 1 standard deviation of the ozone climatology. On panel (e), the average ozone anomaly profile measured by the balloon sondes in Réunion Island is shown in magenta (ozonesonde data degraded to MLS vertical resolution, see Methods). On panels (d) and (e), the dashed orange lines correspond to the ± 1 standard deviation of the HCl climatology, and the dashed blue lines correspond to ± 1 standard deviation of the ClO climatology. The numbers on panels (d) and (e) indicate how many profiles were used to compute the average anomaly. For ClO the averaged anomaly profiles are computed for daytime (in blue) and nighttime (in purple) ClO measurements.

We compute average ozone anomaly and standard error profiles inside the plume for the period 16-24 January for two H_2O thresholds (10 and 100 ppmv) to assess the sensitivity of stratospheric ozone decrease to H_2O conditions (Fig. 2c). The decrease in MLS ozone is more pronounced for higher H_2O mixing ratios, and the largest average ozone drop of 0.4 ppmv (standard error of 0.04 ppmv) at 28 km is observed for profiles with H_2O mixing ratios larger than 100 ppmv. 30% of all 190 ozone profiles selected using the 100 ppmv H_2O mixing ratio threshold show ozone dropping below 0.5 ppmv. This change is larger than the typical range of variability established by MLS ozone measurements for the January 2005-2021 period (standard deviation of 0.25 ppmv) or the 2-σ uncertainty of individual MLS ozone data points (0.1 ppmv) (*20*).

The average ozone decrease in the ozonesonde profiles is 0.6 ppmv (standard error of 0.25 ppmv) near 27-29 km, and the strongest decrease is observed during the night of 22 January, when water vapor mixing ratios were highest. Thus, the large quantity of water vapor injected by the HT volcano appears to have played a key role in the stratospheric ozone decrease observed by both ozonesondes and MLS.

Discussion:

The Mt. Pinatubo eruption in June 1991 decreased the tropical ozone column substantially, by 13-20 Dobson Units (DU) (*7*, *21*) 3 to 6 months after the eruption. This is of similar magnitude to the 18.3 DU loss noted in the January 22 ozone profile (Fig. 3b), but less than a week after the HT eruption. This rapidity of the tropical stratospheric ozone decrease is thus unprecedented. This indicates different mechanisms at play. The low ozone observed in the tropics after the Mt. Pinatubo eruption is likely the result of "lofting" in the tropics (*5*) where the tropical upwelling was accelerated by heating of the volcanic aerosols that ultimately enhanced vertical transport of ozone-poor air from the troposphere to the stratosphere. In the case of the HT eruption, the radiative heating by volcanic aerosols was offset by radiative cooling of the stratosphere from the massive amount of H_2O injected into the stratosphere (*13*), and hence lofting could not have produced that magnitude of ozone loss. Additionally, upward transport at the time of eruption is also not an adequate explanation. A rising volcanic plume can entrain ozone-poor tropospheric air and produce a local column ozone decrease, but this would have resulted in a maximum decrease in the earliest plume observation from MLS on 16 January, as dilution of the volcanic plume would have decreased this apparent loss over time. Minimum ozone values at 27-28 km were observed 5 days after the eruption, therefore, chemical ozone destruction caused by heterogeneous reactions on particles must be considered.

Stratospheric ozone loss inside the HT volcanic plume occurred at rates exceeding those observed in the tropical stratosphere for previous major eruptions such as El Chichòn and Mt. Pinatubo. A drop of 0.5 ppmv for the altitude range 25-29 km was observed less than a week after the HT eruption. For comparison, during the formation of the Antarctic ozone hole, stratospheric ozone at 20 km is destroyed at a rate of about 0.05 ppmv per day (*22*), or about 0.35 ppmv over a comparable period as the HT loss.

Heterogeneous reactions on the particles of polar stratospheric clouds (PSCs) play a key role in polar ozone loss. PSCs, forming at temperatures below ~195 K, provide the surfaces necessary to convert inorganic chlorine (primarily chlorine nitrate, $ClONO_2$ and HCl) to chemically active forms of chlorine (e.g., chlorine monoxide, ClO) (*23*). ClO can then lead to catalytic ozone loss. Experimental studies have shown that these reactions can also occur at higher temperatures (~210 K) on other particle types, including sulfuric acid droplets (*24*). Activation of $ClONO_2$ and HCl via heterogeneous reactions becomes more efficient as temperature decreases, or increased H_2O dilutes the sulfuric acid concentration (*25*).

Modeling studies have indicated that enhanced H_2O in the stratosphere could lead to chemical ozone loss through heterogeneous chlorine activation and subsequent ozone destruction (*17*, *26*). Low temperatures (below 203 K) and elevated H_2O mixing ratios (> 20 ppmv) must be maintained for heterogeneous chlorine activation on sulfate aerosols to occur (*26*).

The largest ozone loss observed above Réunion Island on 22 January 2022 coincides with H_2O mixing ratios exceeding 100 ppmv at ~25 and 27 km (Fig. 3). Above 25 km, temperature values are 2 to 4 K below the climatological mean temperature profile for January computed using 1998-2021 SHADOZ data for Réunion Island (see Methods). Radiosoundings in the tropics have indicated an average temperature decrease of 2 K due to the large increase of water vapor after the HT eruption (*13*). In Fig. 3, ozone decreases also coincide with the presence of aerosols as indicated by peaks in the COBALD backscatter measurements. Measurements from an optical particle counter instrument flown on that night provide additional information on the aerosol size and concentration, from which aerosol surface area density can be estimated (see Methods). In Fig. 3, the aerosol measurements indicate a peak ambient surface area density of 286.9 $\mu m^2\ cm^{-3}$ at 26.4 km. This is 4 to 6 times higher than what was reported after the Mt. Pinatubo eruption (*27*), and ~600 times higher than the background stratospheric value of 0.5 $\mu m^2\ cm^{-3}$. The large humidification of the stratosphere by the HT eruption resulted in rapid aerosol formation in the volcanic plume and the corresponding large aerosol surface area (*16*, *28*).

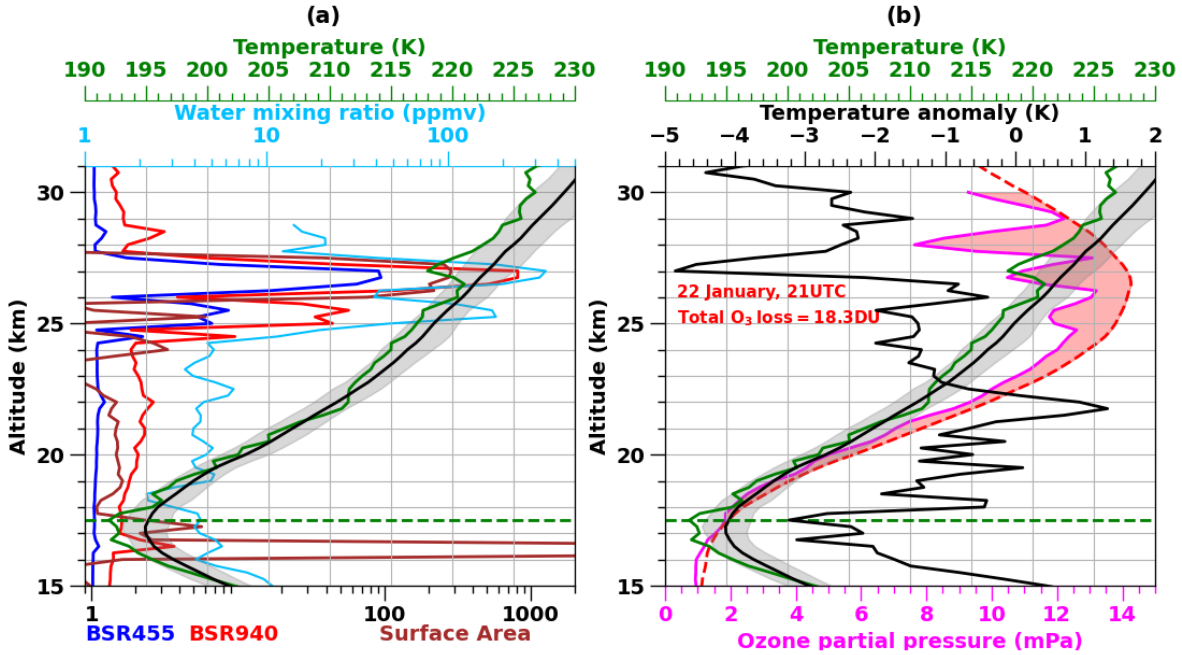

Fig. 3: Soundings at Maïdo Observatory on 22 January. a) Profiles of water vapor mixing ratio (blue), aerosol backscatter ratios at 940 nm (red) and 455 nm (blue), aerosol ambient surface area density (brown, in $\mu m^2\ cm^{-3}$); and b) ozone partial pressure (magenta) and temperature (green) measured at Maïdo Observatory on 22 January 2022. The location of the tropopause is indicated by the horizontal green dashed line and the ozone climatology for Réunion Island corresponds to the red dashed line. The red shaded area illustrates the observed ozone loss estimated for that night. The climatological temperature profile for January 1998-2021 for Réunion Island is in black on panels (a) and (b) as well as the temperature anomaly from the climatology on panel (b). The gray shaded area illustrates the ± 1 standard deviation of the temperature climatology.

The large stratospheric humidification, subsequent radiative cooling and the added surface area likely accelerated heterogeneous chemistry on sulfate aerosols and catalytic ozone loss. MLS measurements at 27 km inside the volcanic plume indicate ozone decreases (average ozone anomaly of -0.4 ppmv with decreases as large as -1.5 ppmv) correlated with higher water vapor (*29*)mixing ratios (mean H_2O of 102 ppmv) and temperatures on average 2 K below the climatology (see Methods; Fig. S1). Above 25 km, where most of the ozone loss is observed, temperatures are usually far too warm (> 220 K) for heterogeneous activation of HCl to ClO to occur (see Methods). However, when water vapor mixing ratios exceed 100 ppmv, the probability of the HCl + $ClONO_2$ reaction increases by 4 orders of magnitude at warm temperatures (see Methods; Fig. S2). The radiative cooling induced by the large amount of water vapor (-4 K from Fig. 3) can further increase this probability by another factor of 10 (see Methods; Fig. S2). An increase in water vapor and corresponding decrease in temperature results in more dilute sulfate aerosols and higher HCl solubility; hence the reaction probability for the conversion of HCl to ClO increases dramatically and catalytic ozone loss becomes possible at relatively warm temperatures.

Although the HCl injection into the stratosphere by the HT eruption was comparable to that from previous moderate eruptions observed during the MLS record (*10*), it reached an altitude near 31.6 hPa (~24 km) on 16-17 January, well above levels previously observed by MLS (*10*). In Fig. 2, two main negative HCl anomalies are observed at 24 and 29 km for measurements with

large water vapor mixing ratios (> 100 ppmv) inside the volcanic plume. The first HCl anomaly value of -0.25 ppbv at 24 km may be due to scavenging by ice or ash particles (*30*), which were injected up to ~23 km but rapidly washed out within the first day following the eruption (*31*). Moreover, experimental studies have indicated that a quasi-liquid layer (QLL) can form rapidly on ice particles at temperatures below the bulk melting point for ice exposed to high HCl and H_2O content (*29*). QLL surfaces mediate chemical reactions at the vapor-ice interface and could have enhanced the chlorine activation reaction of HCl with $ClONO_2$ (*29*) on ice particles inside the volcanic plume. The second, larger HCl anomaly of -0.4 ppbv at 29 km may indicate HCl heterogeneous activation on sulfate aerosols. Indeed, this negative HCl anomaly coincides with a positive peak of 0.41 ppbv in ClO radicals that is much more pronounced for daytime measurements (Fig. 2). Such high ClO radical observations provide direct observational evidence for chlorine activation, consistent with efficient Cl_2 production by the HCl + $ClONO_2$ heterogeneous reac tion on sulfate aerosols at unusually warm temperatures.

The observed catalytic ozone loss is primarily due to an invigorated ClO_x (Cl/ClO) ozone loss catalytic cycle, possibly assisted by other halogens. The chain length in stratospheric ozone depletion cycles can be considered as an estimate of ozone decline via the catalytic cycles (*32*). For the ClOx cycle, a chain length greater than 10 is found in most of the stratosphere (i.e., each ClO molecule produced can lead to the destruction of 10 ozone molecules), which would imply a ratio of 10 or more for ozone to ClO anomaly. Between 20 and 15 hPa, where warmer temperatures make chlorine activation unlikely under baseline conditions, the chain length can range from 50 to 500 (*33*). Inside the HT plume the ratio of peak ozone to ClO anomalies is about 870 (*29*) (0.41 ppmv/0.47 ppbv) in Fig. 2, not inconsistent with the upper range estimate, but 2 to 20 times higher (these values represent a first-order plausibility argument; a large range of ozone and ClO anomalies is observed in the MLS data set). Indeed, this estimate of chain length is a lower limit, since a decrease in NO_2 radical observations indicate slowing of the NO_x cycle, presumably due to N_2O_5 hydrolysis (see Methods; Fig. S3). At sunset NO_2 is higher than in the morning, and better approximates baseline conditions, suggesting that NO_x may at least partially be sustained in the daytime plume. An initial examination of groundbased DOAS observations of BrO radicals in the plume are indistinguishable from clear-sky values before the plume arrival (see Materials), but there is large uncertainty. An invigorated BrO_x cycle at elevated ClO concentrations (i.e., BrO + ClO reaction) could contribute to some ozone loss. No significant impact on ozone by HO_x gas-phase chemistry was seen in a global climate model simulation with enhanced water vapor following the HT eruption (*28*). Similarly, an increase of water vapor in the lower stratosphere did not have an impact on the HO_x cycle expected from humidification and added surface area density (*34*). A full chemical box-model study with Lagrangian modeling (*26*) is needed to better examine the very rapid observed ozone loss in the volcanic plume; such model development is in part limited by uncertainty surrounding chlorine activation (*29*, *35*) associated with supercooled aerosol proxy solutions and ice surfaces under the conditions of the HT plume.

The large amount of seawater vaporized during the eruption contains sea salt that may have been transported to the stratosphere, providing a source of reactive chlorine, bromine, and iodine for ozone destruction. However, it is unclear whether all components of sea salt aerosols would survive wet scavenging in the volcanic plume and be efficiently transported to the stratosphere. Inorganic chlorine (HCl, Cl^-) and bromine (HBr, Br^-) are easily removed by wet scavenging, while iodine is not (*36*). Even a small injection of iodine into the stratosphere could have

accelerated ozone loss in the volcanic plume due to its much larger ozone-depleting efficiency (*36–38*)

Anderson et al. (2012)(*17*) hypothesized that excess mid latitude stratosphere water associated with convection changes due to global warming could destroy lower stratospheric ozone. This HT event appears to be an extreme example of that mechanism. The quantity of water from HT is significantly larger than expected from overshooting monsoon convection but provides observational evidence that this process occurs (see supplement). The rapid chemical ozone loss inside the HT volcanic plume was primarily triggered by the synergistic effects of large humidification, radiative cooling and added aerosol surface area. All effects act in concert to accelerate HCl heterogeneous activation on sulfate aerosols at warmer temperatures than previously studied. The fact that stratospheric ozone loss was so rapid after the HT eruption calls for additional experimental studies of heterogeneous chemistry on hydrated aerosols (especially halogen chemistry) to better assess the kinetics of these reactions. It also identifies the need to develop atmospheric modeling tools at finer scales to better understand stratospheric ozone chemistry in the tropics after extreme events. The increased stratospheric H_2O may linger for 4-5 years, potentially altering ozone chemistry. As noted in Solomon et al. (2022)(*39*) in regards to the Australian New Year bush fires from 2019/2020, which injected 0.9 Tg of smoke into the stratosphere, there were chemical shifts associated with heterogeneous reactions that alter nitrogen, chlorine and reactive hydrogen species with the potential to cause mid latitude ozone loss. For the next few years, continued monitoring is needed of ozone, water vapor, aerosols, and halogens to assess the extended impacts of this unprecedented HT eruption.

References

1. V. Aquila, L. D. Oman, R. S. Stolarski, P. R. Colarco, P. A. Newman, Dispersion of the volcanic sulfate cloud from a Mount Pinatubo-like eruption: dispersion of a Mount Pinatubo cloud. *J. Geophys. Res.* **117** (2012), doi:10.1029/2011JD016968.

2. D. J. Hofmann, S. Solomon, Ozone destruction through heterogeneous chemistry following the eruption of El Chichón. *J. Geophys. Res.* **94**, 5029 (1989).

3. A. Adriani, G. Fiocco, G. P. Gobbi, F. Congeduti, Correlated behavior of the aerosol and ozone contents of the stratosphere after the El Chichon eruption. *J. Geophys. Res.* **92**, 8365 (1987).

4. W. J. Randel, F. Wu, J. M. Russell, J. W. Waters, L. Froidevaux, Ozone and temperature changes in the stratosphere following the eruption of Mount Pinatubo. *J. Geophys. Res.* **100**, 16753 (1995).

5. G. Brasseur, C. Granier, Mount Pinatubo Aerosols, Chlorofluorocarbons, and Ozone Depletion. *Science*. **257**, 1239–1242 (1992).

6. J. K. Angell, Estimated impact of Agung, El Chichon and Pinatubo volcanic eruptions on global and regional total ozone after adjustment for the QBO. *Geophys. Res. Lett.* **24**, 647–650 (1997).

7. M. R. Schoeberl, P. K. Bhartia, E. Hilsenrath, O. Torres, Tropical ozone loss following the eruption of Mt. Pinatubo. *Geophys. Res. Lett.* **20**, 29–32 (1993).

8. S. A. Carn, K. D. Froyd, B. E. Anderson, P. Wennberg, J. Crounse, K. Spencer, J. E. Dibb, N. A. Krotkov, E. V. Browell, J. W. Hair, G. Diskin, G. Sachse, S. A. Vay, *J. Geophys. Res.*, in press, doi:10.1029/2010JD014718.

9. J. L. Carr, Á. Horváth, D. L. Wu, M. D. Friberg, Stereo Plume Height and Motion Retrievals for the Record-Setting Hunga Tonga-Hunga Ha'apai Eruption of 15 January 2022. *Geophysical Research Letters*. **49** (2022), doi:10.1029/2022GL098131.

10. L. Millán, M. L. Santee, A. Lambert, N. J. Livesey, F. Werner, M. J. Schwartz, H. C. Pumphrey, G. L. Manney, Y. Wang, H. Su, L. Wu, W. G. Read, L. Froidevaux, The Hunga Tonga-Hunga Ha'apai Hydration of the Stratosphere. *Geophysical Research Letters*. **49** (2022), doi:10.1029/2022GL099381.

11. W. G. Read, L. Froidevaux, J. W. Waters, Microwave limb sounder measurement of stratospheric SO_2 from the Mt. Pinatubo Volcano. *Geophys. Res. Lett.* **20**, 1299–1302 (1993).

12. G. J. S. Bluth, S. D. Doiron, C. C. Schnetzler, A. J. Krueger, L. S. Walter, Global tracking of the SO2 clouds from the June, 1991 Mount Pinatubo eruptions. *Geophys. Res. Lett.* **19**, 151–154 (1992).

13. H. Vömel, S. Evan, M. Tully, Water vapor injection into the stratosphere by Hunga Tonga-Hunga Ha'apai. *Science*. **377**, 1444–1447 (2022).

14. J.-L. Baray, Y. Courcoux, P. Keckhut, T. Portafaix, P. Tulet, J.-P. Cammas, A. Hauchecorne, S. Godin Beekmann, M. De Mazière, C. Hermans, F. Desmet, K. Sellegri, A. Colomb, M. Ramonet, J. Sciare, C. Vuillemin, C. Hoareau, D. Dionisi, V. Duflot, H. Vérèmes, J. Porteneuve, F. Gabarrot, T. Gaudo, J.-M. Metzger, G. Payen, J. Leclair de Bellevue, C. Barthe, F. Posny, P. Ricaud, A. Abchiche, R. Delmas, Maïdo observatory: a new high-altitude station facility at Reunion Island (21° S, 55° E) for long-term atmospheric remote sensing and in situ measurements. *Atmos. Meas. Tech.* **6**, 2865–2877 (2013).

15. J.-P. Vernier, L. Kalnajs, J. A. Diaz, T. Reese, E. Corrales, A. Alan, H. Vernier, L. Holland, A. Patel, N. Rastogi, F. Wienhold, S. Carn, N. Krotkov, J. Murray, VolKilau: Volcano Rapid Response Balloon Campaign during the 2018 Kilauea Eruption. *Bulletin of the American Meteorological Society*. **101**, E1602–E1618 (2020).

16. E. Asher, M. Todt, K. Rosenlof, T. Thornberry, R.-S. Gao, G. Taha, P. Walter, S. L. Alvarez, J. Flynn, S. M. Davis, S. Evan, J. Brioude, J.-M. Metzger, D. F. Hurst, E. Hall, K. Xiong, Unexpectedly rapid aerosol formation in the Hunga Tonga plume. *Proc. Natl. Acad. Sci. U.S.A.* (2022).

17. J. G. Anderson, D. M. Wilmouth, J. B. Smith, D. S. Sayres, UV Dosage Levels in Summer: Increased Risk of Ozone Loss from Convectively Injected Water Vapor. *Science*. **337**, 835–839 (2012).

18. S. Yoon, A. Kotsakis, S. L. Alvarez, M. G. Spychala, E. Klovenski, P. Walter, G. Morris, E. Corrales, A. Alan, J. A. Diaz, J. H. Flynn, Development and testing of a novel sulfur dioxide sonde. *Atmos. Meas. Tech.* **15**, 4373–4384 (2022).

19. J. W. Waters, L. Froidevaux, R. S. Harwood, R. F. Jarnot, H. M. Pickett, W. G. Read, P. H. Siegel, R. E. Cofield, M. J. Filipiak, D. A. Flower, J. R. Holden, G. K. Lau, N. J. Livesey, G. L. Manney, H. C. Pumphrey, M. L. Santee, D. L. Wu, D. T. Cuddy, R. R. Lay, M. S. Loo, V. S. Perun, M. J. Schwartz, P. C. Stek, R. P. Thurstans, M. A. Boyles, K. M. Chandra, M. C. Chavez, Gun-Shing Chen, B. V. Chudasama, R. Dodge, R. A. Fuller, M. A. Girard, J. H. Jiang, Yibo Jiang, B. W. Knosp, R. C. LaBelle, J. C. Lam, K. A. Lee, D. Miller, J. E. Oswald, N. C. Patel, D. M. Pukala, O. Quintero, D. M. Scaff, W. Van Snyder, M. C. Tope, P. A. Wagner, M. J. Walch, The Earth observing system microwave limb sounder (EOS MLS) on the aura Satellite. *IEEE Trans. Geosci. Remote Sensing*. **44**, 1075–1092 (2006).

20. N. J. Livesey, W. G. Read, P. A. Wagner, L. Froidevaux, A. Lambert, G. L. Manney, L. F. M. Valle, H. C. Pumphrey, M. L. Santee, M. J. Schwartz, S. Wang, R. A. Fuller, R. F. Jarnot, B. W. Knosp, E. Martinez, R. R. Lay, "EOS MLS Version 4.2x Level 2 data quality and description document (Revision E)" (Technical Report, 2020), (available at https://mls.jpl.nasa.gov/eos-aura-mls/data-documentation).

21. W. B. Grant, J. Fishman, E. V. Browell, V. G. Brackett, D. Nganga, A. Minga, B. Cros, R. E. Veiga, C. F. Butler, M. A. Fenn, G. D. Nowicki, Observations of reduced ozone concentrations in the tropical stratosphere after the eruption of Mt. Pinatubo. *Geophys. Res. Lett.* **19**, 1109–1112 (1992).

22. S. Solomon, Progress towards a quantitative understanding of Antarctic ozone depletion. *Nature*. **347**, 347–354 (1990).

23. S. Solomon, Stratospheric ozone depletion: A review of concepts and history. *Rev. Geophys.* **37**, 275–316 (1999).

24. M. A. Tolbert, M. J. Rossi, R. Malhotra, D. M. Golden, Reaction of Chlorine Nitrate with Hydrogen Chloride and Water at Antarctic Stratospheric Temperatures. *Science*. **238**, 4 (1987).

25. M. A. Tolbert, M. J. Rossi, D. M. Golden, Heterogeneous interactions of chlorine nitrate, hydrogen chloride, and nitric acid with sulfuric acid surfaces at stratospheric temperatures. *Geophys. Res. Lett.* **15**, 847–850 (1988).

26. S. Robrecht, B. Vogel, J.-U. Grooß, K. Rosenlof, T. Thornberry, A. Rollins, M. Krämer, L. Christensen, R. Müller, Mechanism of ozone loss under enhanced water vapour conditions in the mid-latitude lower stratosphere in summer. *Atmos. Chem. Phys.* **19**, 5805–5833 (2019).

27. T. Deshler, D. J. Hofmann, B. J. Johnson, W. R. Rozier, Balloonborne measurements of the Pinatubo aerosol size distribution and volatility at Laramie, Wyoming during the summer of 1991. *Geophys. Res. Lett.* **19**, 199–202 (1992).

28. Y. Zhu, C. G. Bardeen, S. Tilmes, M. J. Mills, X. Wang, V. L. Harvey, G. Taha, D. Kinnison, R. W. Portmann, P. Yu, K. H. Rosenlof, M. Avery, C. Kloss, C. Li, A. S. Glanville, L. Millán, T. Deshler, N. Krotkov, O. B. Toon, Perturbations in stratospheric aerosol evolution due to the water-rich plume of the 2022 Hunga-Tonga eruption. *Commun Earth Environ*. **3**, 248 (2022).

29. V. F. McNeill, T. Loerting, F. M. Geiger, B. L. Trout, M. J. Molina, Hydrogen chloride-induced surface disordering on ice. *Proc. Natl. Acad. Sci. U.S.A.* **103**, 9422–9427 (2006).

30. A. Tabazadeh, R. P. Turco, Stratospheric Chlorine Injection by Volcanic Eruptions: HCl Scavenging and Implications for Ozone. *Science*. **260**, 1082–1086 (1993).

31. B. Legras, C. Duchamp, P. Sellitto, A. Podglajen, E. Carboni, R. Siddans, J.-U. Grooß, S. Khaykin, F. Ploeger, "The evolution and dynamics of the Hunga Tonga plume in the stratosphere" (preprint, Dynamics/Remote Sensing/Stratosphere/Physics (physical properties and processes), 2022), , doi:10.5194/egusphere-2022-517.

32. D. J. Lary, Catalytic destruction of stratospheric ozone. *J. Geophys. Res.* **102**, 21515–21526 (1997).

33. O. Morgenstern, K. A. Stone, R. Schofield, H. Akiyoshi, Y. Yamashita, D. E. Kinnison, R. R. Garcia, K. Sudo, D. A. Plummer, J. Scinocca, L. D. Oman, M. E. Manyin, G. Zeng, E. Rozanov, A. Stenke, L. E. Revell, G. Pitari, E. Mancini, G. Di Genova, D. Visioni, S. S. Dhomse, M. P. Chipperfield, Ozone sensitivity to varying greenhouse gases and ozone-depleting substances in CCMI-1 simulations. *Atmos. Chem. Phys.* **18**, 1091–1114 (2018).

34. J. G. Anderson, D. K. Weisenstein, K. P. Bowman, C. R. Homeyer, J. B. Smith, D. M. Wilmouth, D. S. Sayres, J. E. Klobas, S. S. Leroy, J. A. Dykema, S. C. Wofsy, Stratospheric ozone over the United States in summer linked to observations of convection and temperature via chlorine and bromine catalysis. *Proc. Natl. Acad. Sci. U.S.A.* **114** (2017), doi:10.1073/pnas.1619318114.

35. A. Bogdan, M. J. Molina, H. Tenhu, E. Mayer, T. Loerting, Formation of mixed-phase particles during the freezing of polar stratospheric ice clouds. *Nature Chem*. **2**, 197–201 (2010).

36. T. K. Koenig, S. Baidar, P. Campuzano-Jost, C. A. Cuevas, B. Dix, R. P. Fernandez, H. Guo, S. R. Hall, D. Kinnison, B. A. Nault, K. Ullmann, J. L. Jimenez, A. Saiz-Lopez, R. Volkamer, Quantitative detection of iodine in the stratosphere. *Proc. Natl. Acad. Sci. U.S.A.* **117**, 1860–1866 (2020).

37. L. J. Carpenter, S. Reimann, J. B. Burkholder, C. Clerbaux, B. D. Hall, R. Hossaini, J. C. Laube, S. A. Yvon-Lewis, Update on ozone-depleting substances (ODSs) and other gases of interest to the Montreal protocol. *9789966076014* (2014).

38. "World Meteorological Organization (WMO). Executive Summary. Scientific Assessment of Ozone Depletion: 2022" (GAW Report No. 278, WMO: Geneva, 2022), p. 56.

39. S. Solomon, K. Dube, K. Stone, P. Yu, D. Kinnison, O. B. Toon, S. E. Strahan, K. H. Rosenlof, R. Portmann, S. Davis, W. Randel, P. Bernath, C. Boone, C. G. Bardeen, A. Bourassa, D. Zawada, D. Degenstein, On the stratospheric chemistry of midlatitude wildfire smoke. *Proc. Natl. Acad. Sci. U.S.A.* **119**, e2117325119 (2022).

40. H. Vömel, J. E. Barnes, R. N. Forno, M. Fujiwara, F. Hasebe, S. Iwasaki, R. Kivi, N. Komala, E. Kyrö, T. Leblanc, B. Morel, S.-Y. Ogino, W. G. Read, S. C. Ryan, S. Saraspriya, H. Selkirk, M. Shiotani, J. Valverde Canossa, D. N. Whiteman, *J. Geophys. Res.*, in press, doi:10.1029/2007JD008698.

41. H. Vömel, T. Naebert, R. Dirksen, M. Sommer, An update on the uncertainties of water vapor measurements using cryogenicfrost point hygrometers. *Atmos. Meas. Tech.* **9**, 3755–3768 (2016).

42. M. Brabec, F. G. Wienhold, B. P. Luo, H. Vömel, F. Immler, P. Steiner, E. Hausammann, U. Weers, T. Peter, Particle backscatter and relative humidity measured across cirrus clouds and comparison with microphysical cirrus modelling. *Atmos. Chem. Phys.* **12**, 9135–9148 (2012).

43. S. Brunamonti, T. Jorge, P. Oelsner, S. Hanumanthu, B. B. Singh, K. R. Kumar, S. Sonbawne, S. Meier, D. Singh, F. G. Wienhold, B. P. Luo, M. Boettcher, Y. Poltera, H. Jauhiainen, R. Kayastha, J. Karmacharya, R. Dirksen, M. Naja, M. Rex, S. Fadnavis, T. Peter, Balloon-borne measurements of temperature, water vapor, ozone and aerosol backscatter on the southern slopes of the Himalayas during StratoClim 2016–2017. *Atmos. Chem. Phys.* **18**, 15937–15957 (2018).

44. A. Bucholtz, Rayleigh-scattering calculations for the terrestrial atmosphere. *Appl. Opt.* **34**, 2765 (1995).

45. J. -P. Vernier, T. D. Fairlie, M. Natarajan, F. G. Wienhold, J. Bian, B. G. Martinsson, S. Crumeyrolle, L. W. Thomason, K. M. Bedka, Increase in upper tropospheric and lower stratospheric aerosol levels and its potential connection with Asian pollution. *J. Geophys. Res. Atmos.* **120**, 1608–1619 (2015).

46. R. S. Gao, H. Telg, R. J. McLaughlin, S. J. Ciciora, L. A. Watts, M. S. Richardson, J. P. Schwarz, A. E. Perring, T. D. Thornberry, A. W. Rollins, M. Z. Markovic, T. S. Bates, J. E. Johnson, D. W. Fahey, A light-weight, high-sensitivity particle spectrometer for PM2.5 aerosol measurements. *Aerosol Science and Technology*. **50**, 88–99 (2016).

47. W. Komhyr, Electrochemical concentration cells for gas analysis. *ANNALES DE GEOPHYSIQUE*. **25**, 203–210 (1969).

48. Smit, Herman G. J., A. M. Thompson, ASOPOS 2.0 Panel, "Ozonesonde Measurement Principles and Best Operational Practices: ASOPOS 2.0 (Assessment of Standard Operating Procedures for Ozonesondes) August 2021" (GAW report 268, WMO, 2021), (available at https://library.wmo.int/doc_num.php?explnum_id=10884).

49. J. C. Witte, A. M. Thompson, H. G. J. Smit, M. Fujiwara, F. Posny, G. J. R. Coetzee, E. T. Northam, B. J. Johnson, C. W. Sterling, M. Mohamad, S.-Y. Ogino, A. Jordan, F. R. da

Silva, First reprocessing of Southern Hemisphere ADditional OZonesondes (SHADOZ) profile records (1998-2015): 1. Methodology and evaluation: SHADOZ Reprocessed Ozonesonde Profiles. *J. Geophys. Res. Atmos.* **122**, 6611–6636 (2017).

50. J. C. Witte, A. M. Thompson, H. G. J. Smit, H. Vömel, F. Posny, R. Stübi, First Reprocessing of Southern Hemisphere ADditional OZonesondes Profile Records: 3. Uncertainty in Ozone Profile and Total Column. *JGR Atmospheres*. **123**, 3243–3268 (2018).

51. A. M. Thompson, J. C. Witte, C. Sterling, A. Jordan, B. J. Johnson, S. J. Oltmans, M. Fujiwara, H. Vömel, M. Allaart, A. Piters, G. J. R. Coetzee, F. Posny, E. Corrales, J. A. Diaz, C. Félix, N. Komala, N. Lai, H. T. Ahn Nguyen, M. Maata, F. Mani, Z. Zainal, S. Ogino, F. Paredes, T. L. B. Penha, F. R. Silva, S. Sallons-Mitro, H. B. Selkirk, F. J. Schmidlin, R. Stübi, K. Thiongo, First Reprocessing of Southern Hemisphere Additional Ozonesondes (SHADOZ) Ozone Profiles (1998–2016): 2. Comparisons with Satellites and Ground-Based Instruments. *J. Geophys. Res. Atmos.* **122** (2017), doi:10.1002/2017JD027406.

52. W. G. Read, A. Lambert, J. Bacmeister, R. E. Cofield, L. E. Christensen, D. T. Cuddy, W. H. Daffer, B. J. Drouin, E. Fetzer, L. Froidevaux, R. Fuller, R. Herman, R. F. Jarnot, J. H. Jiang, Y. B. Jiang, K. Kelly, B. W. Knosp, L. J. Kovalenko, N. J. Livesey, H.-C. Liu, G. L. Manney, H. M. Pickett, H. C. Pumphrey, K. H. Rosenlof, X. Sabounchi, M. L. Santee, M. J. Schwartz, W. V. Snyder, P. C. Stek, H. Su, L. L. Takacs, R. P. Thurstans, H. Vömel, P. A. Wagner, J. W. Waters, C. R. Webster, E. M. Weinstock, D. L. Wu, *J. Geophys. Res.*, in press, doi:10.1029/2007JD008752.

53. S. M. Davis, K. H. Rosenlof, B. Hassler, D. F. Hurst, W. G. Read, H. Vömel, H. Selkirk, M. Fujiwara, R. Damadeo, The Stratospheric Water and Ozone Satellite Homogenized (SWOOSH) database:a long-term database for climate studies. *Earth Syst. Sci. Data*. **8**, 461–490 (2016).

54. G. A. Morris, W. D. Komhyr, J. Hirokawa, J. Flynn, B. Lefer, N. Krotkov, F. Ngan, A Balloon Sounding Technique for Measuring SO2 Plumes. *Journal of Atmospheric and Oceanic Technology*. **27**, 1318–1330 (2010).

55. S. Coburn, B. Dix, R. Sinreich, R. Volkamer, The CU ground MAX-DOAS instrument: characterization of RMS noise limitations and first measurements near Pensacola, FL of BrO, IO, and CHOCHO. *Atmos. Meas. Tech.* **4**, 2421–2439 (2011).

56. M. R. Bassford, C. A. McLinden, K. Strong, Zenith-sky observations of stratospheric gases: the sensitivity of air mass factors to geophysical parameters and the influence of tropospheric clouds. *Journal of Quantitative Spectroscopy and Radiative Transfer*. **68**, 657–677 (2001).

57. Q. Shi, J. T. Jayne, C. E. Kolb, D. R. Worsnop, P. Davidovits, Kinetic model for reaction of $ClONO_2$ with H_2O and HCl and HOCl with HCl in sulfuric acid solutions. *J. Geophys. Res.* **106**, 24259–24274 (2001).

58. D. R. Hanson, Reaction of ClONO2 with H2O and HCl in sulfuric acid and HNO3/H2SO4/H2O mixtures. *The Journal of Physical Chemistry A*. **102**, 4794–4807 (1998).

Acknowledgments: The authors acknowledge the European Communities, the Région Réunion, CNRS and Université de la Réunion for their support and contributions in the construction phase of the research infrastructure OPAR (Observatoire de Physique de l'Atmosphère de La Réunion, including Maïdo Observatory). OPAR is presently funded by CNRS (INSU), Météo France, and Université de La Réunion and managed by OSU- R (Observatoire des Sciences de l'Univers de La Réunion, UAR 3365). We thank Gary Morris, Daniel Murphy, Maya Abou-Ghane and Jim Burkholder for their discussions. We also thank Alex Wong and SilverLining for their support.

Funding :

Agence Nationale de la Recherche (ANR) CONCIRTO award ANR-17-CEO1-0005-01.

National Science Foundation (NSF) awards AGS-1620530 and AGS-2027252.

National Aeronautics and Space Administration (NASA) contract 80NM0018D0004.

Author contributions:

Conceptualization: SE

Methodology: SE, JB,

Data curation: SE, JB, RV, CFL, JMM, KL, PW, SLA, JHF, EA, MT, LA, MT, PW, SA, HV, FGW, LM, MLS, LF, WGR

Writing – original draft: SE, JB, KHR, RG, RWP, RV, CFL, JMM, KL, PW, SLA, JHF, EA, MT, SMD, TT, HV, FGW, RMS, LM, MLS, LF, WGR

Competing interests: The authors declare no competing interests.

Data and materials availability:

The processed CFH, ECC ozonesonde and COBALD data used in this study are available at https://lacy.univ-reunion.fr/activites/programmes-de-recherche/anr-concirto/donnees.
Raw MLS H_2O, O_3, HCl and ClO data may be found at:
https://disc.gsfc.nasa.gov/datasets/ML2H2O_004/summary?keywords=aura
https://disc.gsfc.nasa.gov/datasets/ML2O3_004/summary?keywords=aura
https://disc.gsfc.nasa.gov/datasets/ML2HCL_004/summary?keywords=aura
https://disc.gsfc.nasa.gov/datasets/ML2CLO_004/summary?keywords=aura

Supplementary Materials:

Data and Methods

Figs. S1 to S3

Tables S1

Science
AAAS

Supplementary Materials for

Rapid ozone loss following humidification of the stratosphere by the Hunga Tonga Eruption

Stephanie Evan[1*], Jerome Brioude[1], Karen H. Rosenlof[2], Ru-Shan Gao[2], Robert W. Portmann[2], Rainer Volkamer[3], Christopher F. Lee[3], Jean-Marc Metzger[4], Kevin Lamy[1], Paul Walter[5], Sergio L. Alvarez[6], James H. Flynn[6], Elizabeth Asher[2,7], Michael Todt[2,7], Sean M. Davis[2], Troy Thornberry[2], Holger Vömel[8], Frank G. Wienhold[9], Ryan M. Stauffer[10], Luis Millán[11], Michelle L. Santee[11], Lucien Froidevaux[11], William G. Read[11]

Correspondence to: stephanie.evan@univ-reunion.fr

This PDF file includes:

Materials and Methods

In situ balloon-borne measurements

We have performed balloon-borne measurements of water vapor, ozone, and aerosols for 5 consecutive nights at the Maïdo Observatory (21.08°S, 55.38°E) on Réunion Island during the period 20-25 January 2022 following the eruption of the Hunga Tonga volcano on 15 January. Réunion Island is in the Southwest Indian Ocean and holds one of the very few atmospheric observatories in the subtropical Southern Hemisphere.

On some of the balloon payloads, a cryogenic frost-point hygrometer (CFH), a Compact Optical Backscatter and AerosoL Detector (COBALD) and an electrochemical concentration cell (ECC) ozonesonde were flown together. Data from the COBALD, CFH and ozone sondes were telemetered to the ground by an Intermet iMet-4-RSB meteorological radiosonde, which additionally provided measurements of ambient pressure, temperature, Global Positioning System

(GPS) altitude, relative humidity (RH), wind speed and direction. Some of the balloon payloads included a SO_2 sonde, an ECC ozonesonde, and a Portable Optical Particle Counter (POPS): a light-weight particle counter designed for aerosol particle size distribution measurements. Table S1 below provides a summary of the measurements schedule.

The CFH was developed to provide highly accurate water vapor measurements in the tropopause region and stratosphere where the water vapor mixing ratios are extremely low (~2 ppmv). CFH mixing ratio measurement uncertainty ranges from 5% in the tropical lower troposphere to less than 10% in the stratosphere (*40*); a recent study shows that the uncertainty in the stratosphere can be as low as 2%–3% (*41*).

The COBALD backscatter instrument, developed at ETH (Swiss Federal Institute of Technology, Zurich), uses two light-emitting diodes at two wavelengths (455 and 940 nm) to detect and characterize cloud and aerosol particles in the atmosphere(*42*)·(*43*). The optical detector has a field of view of ±6°, and the signal detected typically originates from a 0.5–10 m distance from the sonde. Beyond 10 m, the signal contribution becomes negligible. For each of the two COBALD wavelengths, the COBALD raw signal is converted to backscatter ratio (BSR), which is defined as: $BSR = \beta_{tot}/\beta_{mol} = (\beta_{mol}+\beta_{part})/\beta_{mol} = 1 + PBSR$, where PBSR is the particle BSR; β_{tot} is the measured backscatter coefficient, expressed as the sum of the molecular (β_{mol}) and particle (β_{part}) contributions. The particle backscatter coefficient includes scattering of aerosols or ice crystals in the atmosphere. The molecular backscatter coefficient β_{mol} is computed according to ref. (*44*) based on the concurrent radiosonde readings of temperature and pressure. The COBALD sonde has been used to detect and characterize aerosol layers in the upper troposphere–lower stratosphere (*45*).

The POPS instrument (*46*), developed at the National Oceanic and Atmospheric Administration (NOAA) and the Cooperative Institute for Research in Environmental Sciences (CIRES) is an optical particle counter made from a three-dimensional printer to reduce weight (~900 g). It uses a laser at 405nm to measure the backscattering of aerosols crossing the laser path. Based on the backscattering Mie theory, and an assumption on the aerosol particle index of 1.45 valid for sulfate aerosols, POPS can resolve the size of aerosols from 140 nm to 2.5μm with a resolution of 5%. The particle size represents the aerosol dry diameter, since the enclosure temperature is much larger than the ambient air. The surface area of aerosols measured by POPS is calculated using the kappa-Köhler theory that is based on the aerosol dry diameter and ambient relative humidity.

The ECC ozonesonde is often used worldwide to provide accurate measurements of ozone profiles. The ECC ozonesonde generates an electrical current through the reaction of ozone in a potassium iodide sensing solution, which produces approximately two electrons per molecule of ozone (*47*). The ozone partial pressure (P_{O_3}) is then calculated using the measured cell current I_M.

$$P_{O_3} = \frac{R}{2*F} * \frac{T_P}{\eta_p * \eta_a * \eta_c * \Phi_{P_0}} * (I_M - I_B)$$ (ref.(*48*))

where P_{O_3} is in millipascals, R is the universal gas constant (=8.314 J K^{-1} $mole^{-1}$), F is Faraday's constant (= 9.6487×10^4 C $mole^{-1}$), I_M is the cell current in microamperes attributed to the reaction of ozone with iodide, I_B is the cell background current in microamperes, T_P is the air temperature entering the cell in kelvin, approximated by the temperature of the pump, η_p is the pump flow efficiency as a function of pressure, η_a is the absorption efficiency for the transfer of the sampled gaseous ozone into the liquid phase, η_c is the conversion efficiency of the absorbed ozone in the

cathode sensing solution into iodine and Φ_{P_0} (in $cm^3\ s^{-1}$) is the gas volume flow rate of the air sampling pump.

We follow the guidelines from the Southern Hemisphere ADditional OZonesondes (SHADOZ, (*49–51*)) network to process the ozonesonde data obtained at the Maïdo Observatory. Witte et al. (2017)(*49*) describe corrections of P_{O_3} which includes a conversion efficiency term, a correction for pump flow rate term dependent on the relative humidity and temperature of the laboratory during pre-flight preparation and a pump flow efficiency term which is pressure dependent. Witte et al. (2018) (*50*) estimate that the ECC ozonesonde has an uncertainty of 10% in the tropical stratosphere for austral summer conditions (December to February).

SHADOZ ozonesondes are launched from the airport (Roland Garros; 21.06°S, 55.48°E), located on the north side of the island since 1998. The flying distance between the Maïdo Observatory and the airport is ~20 km. The climatological P_{O_3}mean profile for January used the SHADOZ ozonesonde data from the airport.

At the one per second telemetry data rate, the CFH, COBALD, and ECC ozonesonde data have a high vertical resolution of 5 m with a mean balloon ascent rate of 5 m s^{-1} on most flights. We use the GPS altitude measured by Intermet iMet-4-RSB radiosondes as the main vertical coordinate for all instruments. All variables are binned in altitude intervals of 100 m to reduce measurement noise.

MLS observations and comparison to high-resolution ozonesonde measurements.

The Aura Microwave Limb Sounder (MLS) is a satellite instrument launched by NASA on 15 July 2004. Aura is in a sun-synchronous orbit at an altitude of ~705 km with an inclination angle of 98.2° to the equator, performing approximately 14.5 orbits per day (*19*). MLS observes thermal emission from the atmosphere day and night over a latitude range of 82°S to 82°N. From the measured radiances, profiles of temperature, various trace gases, and cloud ice are retrieved (*19*). As recommended by ref. (*10*), MLS version 4 data are used instead of the most recent version 5. This is because in version 4, pointing information is obtained solely from O_2 signals, while version 5 also uses the H_2O line, affecting the pointing information inside the HT plume. As a result, substantial discrepancies in pointing degrade the accuracy of some version 5 MLS products. The vertical resolution is typically 3 km in the stratosphere up to 10 hPa. We use measurements of H_2O, O_3, HCl, and ClO. MLS measurements inside the volcanic plume are identified by selecting data points which have water vapor mixing ratios above 10 ppmv between 100 and 10 hPa. Then for each data point, the climatological January 2005-2021 average profile is computed by using MLS profiles in a 5°x5° box region around the point.

The estimated accuracy for MLS version 4 O_3 is 5% at 21 hPa. In Fig. 2a, all O_3 data points meet the screening criteria described in the MLS data quality document (*20*). These criteria are indicative of how well the retrieved profiles fit the observed atmospheric microwave spectra. Most of the O_3 data points did pass the MLS quality screening, indicating that the low O_3 values retrieved after the eruption are valid measurements. In Fig. 2b-c, MLS HCl and ClO profiles in the HT volcanic plume have passed the quality screening criteria described in ref. (*20*).

MLS O_3, HCl and ClO averaged anomaly profiles for the period 16-24 January shown in Fig. 2d) and e) are anomalies from the MLS January 2005-2021 climatological profile computed at each data point. We select data points inside the plume corresponding to different water vapor mixing ratio conditions between 100 and 10 hPa (i.e., above 10 and 100 ppmv) to compute the anomaly profiles. This is to assess whether O_3, HCl and ClO anomalies are more pronounced for larger stratospheric water vapor amounts. For ClO, we further examine separately the day and night retrievals. MLS ClO retrievals may be affected by SO_2 interference (*10*). However, that SO_2 contamination is more important at lower levels (i.e., higher pressures), where spectral lines are broader; at the altitudes where the ozone loss is occurring (above ~27 km or 21 hPa), the lines are much narrower, so the SO_2 signal impinges less on the ClO line. Also, if the ClO enhancements in the volcanic plume occur mostly for the daytime MLS measurements (and they do), this indicates that contamination by SO_2 is minimal (as contamination should impact the nighttime data as well as the daytime data).

MLS version 4 O_3 mixing ratio values are reported on pressure levels spaced at 12 levels per pressure decade, a spacing of about 2.7 km in altitude. To compare the high-resolution ozonesonde mixing ratio profile to the MLS satellite data, we smooth the high-resolution sonde measurements to match the resolution of the satellite profiles. First, we compute a least squares fit of the ozonesonde balloon data to the lower-resolution MLS retrieval grid (*20*). Then we apply the MLS vertical averaging kernels, following the procedure described in ref. (*52*) and ref. (*53*). The procedure for applying the MLS averaging kernels to an ozonesonde profile requires an a priori profile as input; for this, we used the climatological January-February 1998-2021 average of SHADOZ ozone mixing ratio profiles for Réunion Island.

Ozonesonde and SO_2 interference

The presence of SO_2 in the air can lead to significant negative interferences in the measurements of ECC ozonesondes. In the ECC ozonesonde, ambient air with ozone is pumped into a cathode chamber that contains a platinum electrode immersed in a low concentration potassium iodide (KI) solution. O_3 molecules react with the KI molecules to produce iodine (I_2). The iodine in contact with the platinum electrode is converted to iodide (I^-) through the uptake of two electrons per molecule of iodine. To rebalance the cathode chamber, the anode chamber with higher concentration KI solution provides electrons via an ion bridge to the cathode. The electrical cell current generated and measured by the ozonesonde is thus directly related to the uptake rate of ozone in the cathode chamber(*47*). The cathode chamber chemistry is altered if SO_2 is present in the air. As a reducing agent, SO_2 converts the produced iodide (I^-) from the ozone/KI reaction back to iodine. This results in a lower cell current measured by the ECC ozonesonde, which reports O_3 concentration minus SO_2 concentration (*54*). Therefore, O_3 values reported by the ECC ozonesondes after the HT eruption can be lower than actual values in the atmosphere if significant SO_2 is present. To account for this SO_2 interference, we need to subtract from the reported depleted O_3 column the actual SO_2 column. During the rapid response experiment, SO_2 instruments (*18*) were launched in tandem with ECC ozonesondes and sampled SO_2 in the stratospheric volcanic plume during four flights. The flight on 21 January 2022, 19:15 UTC, reported a column SO_2 of 0.21 DU between the GPS altitudes of 27.5 and 30.1 km, where the reported O_3 column decrease is 6 DU. An estimated 3-4% (upper limit < 9%) of the ozone partial pressure decrease between 28 and 30 km in the ozonesonde ozone profile on 21 January is thus accounted for by SO_2 interference.

Zenith-Sky DOAS measurements of stratospheric NO_2

Measurements of stratospheric NO_2 during the plume period (21 Jan to 1 Feb 2022) are compared with the clear-sky interannual NO_2 variability for three years (January 2020, 2021, 1-20 Jan 2022) above Maido Observatory (see Fig. S3) to assess whether the NO_x-cycle of stratospheric O_3 destruction was significantly impacted by N_2O_5 hydrolysis in the humidified plume. The University of Colorado Differential Optical Absorption Spectroscopy instrument(*55*) has been operational at Maido Observatory since March 2018. Here, we present twilight (solar zenith angle, SZA > 74 degrees) zenith-sky NO_2 differential Slant Column Densities (dSCDs) retrieved from a 425-465 nm spectral fit window, with fit settings otherwise adapted from the Network for the Detection of Atmospheric Composition Change (NDACC). These measurements present qualitative evidence for a reduction in stratospheric NO_2 during sunrise and sunset, consistent with N_2O_5 hydrolysis; both geometries overlap with the plume. During sunset, NO_2 dSCDs are higher than during sunrise also in the plume, and the delta NO_2 dSCDs (bottom panel) are closer to the clear sky interannual mean. The NO_2 decrease compared to the interannual mean cannot be explained by volcanic aerosols, which would increase the NO_2 dSCDs for SZA < 90 deg (*56*). The largest NO_2 decrease is observed at SZA > 88 deg, consistent with the plume height. Some decrease in the NO_2 dSCD at lower SZA is expected due to the broad vertical sensitivity of zenith-sky DOAS measurements (averaging kernel full-width-half-maximum at 28 km is ~10 km). BrO radicals were also detected by the DOAS before and after the HT plume arrival. No significant difference in the SZA dependence of BrO dSCDs was observed comparing sunrise and sunset data before and after the HT plume arrival (not shown). No evidence for enhanced BrO due to the volcanic plume injection was detectable in the DOAS data.

Heterogeneous chemistry under enhanced water vapor conditions.

The added aerosol surface area and large humidification of the stratosphere after the HT eruption may have affected heterogeneous chemistry on sulfate aerosols. In addition, the increase in water vapor resulted in radiative cooling of the stratosphere (*13*). Fig. S1 displays MLS ozone anomalies at 27 km inside the volcanic plume as a function of temperature and water vapor for the 16-24 January period. The ozone anomalies are relative to the January 2005-2021 MLS ozone climatology computed at each MLS measurement inside the volcanic plume (shown on Figure 2a and selected using the 10 ppmv water vapor mixing ratio threshold). For each ozone anomaly, we keep the coincident MLS measurements of water vapor mixing ratio and temperature (the temperature profiles passed the MLS quality screening criteria), which results in the distribution of ozone anomalies as a function of water vapor and temperature shown in Fig. S1. In Fig. S1, negative ozone anomalies are more pronounced for higher water vapor mixing ratios and lower temperatures. 40% of MLS measurements inside the volcanic plume have negative ozone anomalies, with values as low as -1.5 ppmv. Negative ozone anomalies at 27 km are associated with a mean water vapor of 102 ppmv and temperature of 219 K (2K below the January 2005-2021 temperature climatology for 0-30°S). Thus, ozone decreases inside the volcanic plume are correlated with higher water vapor mixing ratios and lower temperatures (due in part to radiative cooling).

To further assess the effects of humidification and radiative cooling on heterogeneous chemistry, we look at changes in reactive uptake coefficient γ (the probability that a molecule impacting the aerosol surface undergoes reaction) of the $HCl + ClONO_2 \rightarrow HNO_3 + Cl_2$ chemical reaction. Computed γ values for $HCl + ClONO_2$ are based on a parameterization of heterogeneous reactions

and uptake coefficients implemented in the Community Earth System Model (CESM) Whole Atmosphere Community Climate Model (WACCM). The parameterization of γ values is based on ref. (*57*) and is valid for uptake of HCl on sulfate aerosols (binary H_2SO4/H_2O solution) from 185 to 260 K. The formulation of γ developed in ref. (*57*) builds on initial work by ref. (*58*) to include the effects of temperature and partial pressure of water vapor on acid concentration and Henry's law solubilities of HCl and $ClONO_2$. Further details and information on the formulation of uptake coefficients for HCl + $ClONO_2$ are provided in Table A3 of ref. (*57*).

Fig. S2 displays computed γ values for HCl + $ClONO_2$ as a function of temperature between 210 and 230 K at 20 hPa (27 km) for an aerosol radius of 0.3 μm (mean size reported by the POPS instrument on 22 January); 5, 100 and 350 ppmv of water vapor; 1 and 2 ppbv of HCl (range observed on Figure 2b); and 0.5 ppbv of $ClONO_2$. The lower range of water vapor corresponds to background stratospheric water vapor conditions, while 350 ppmv corresponds to the maximum water vapor mixing ratio observed at 27 km inside the volcanic plume on 22 January (Fig. 3). At this altitude, the climatological temperature for January 1998-2021 is 222 K, while the temperature observed on that night is 218 K (Fig. 3).

Under usual background stratospheric water vapor conditions (5 ppmv), the probability of the HCl + $ClONO_2$ heterogeneous reaction at 20 hPa is quite low ($\gamma \sim 1.9\times10^{-9}$) at 222 K. This is far too warm for heterogeneous processing to occur under typical stratospheric conditions. Under vastly perturbed conditions in stratospheric water vapor as observed after the HT eruption, γ values for HCl + $ClONO_2$ increase by 4 orders of magnitude to reach 7.2×10^{-5} when water vapor reaches 350 ppmv at 222 K. Thus, water vapor injection into the stratosphere by the HT volcano increases the probability of heterogeneous processing of HCl to occur, even at warm stratospheric temperatures. The radiative cooling induced by the large amount of water vapor (-4 K in Figure 3) can further increase γ values by a factor of 10 to reach 5.7×10^{-4}. Increasing the amount of HCl has a relatively smaller effect as γ values are doubled when HCl increases from 1 to 2 ppbv. At lower pressure (15 hPa), γ values are smaller but still in the 10^{-5} to 10^{-4} range ($\gamma = 1.7\times10^{-4}$ for H_2O = 350 ppmv, HCl = 1 ppbv, T = 218 K). Overall, the probability of the HCl + $ClONO_2$ heterogeneous reaction on sulfate aerosols increases under the unusual stratospheric water vapor/temperature conditions encountered after the HT eruption. An increase in water vapor and corresponding decrease in temperature due to radiative cooling results in more dilute sulfate within the aerosol, and as a result the solubility of HCl increases. With shifts to higher water vapor mixing ratios and lower temperatures, the reaction probability for the conversion of HCl to ClO increases significantly and catalytic ozone loss becomes possible at relatively warm temperatures.

We can compute the time for removal of HCl via heterogeneous chemistry on sulfate aerosols according to ref. (*2*). The characteristic time τ_{HCl} (in seconds) for the deposition of HCl on sulfate aerosols can be expressed as $\tau_{HCl}{}^{-1} = \gamma \upsilon A/4$, where γ is the uptake coefficient, υ is the average molecular velocity (cm s^{-1}) and A is the aerosol surface area density (cm ^{2} cm^{-3}). The maximum surface area density of 2.9×10^{-6} cm ^{2} cm^{-3} was observed at 27 km on 22 January. In Extended Figure 2, the γ value for HCl + $ClONO_2$ is about 5.7×10^{-4} at 20 hPa for conditions inside the volcanic plume (H_2O = 350 ppmv, T = 218 K, HCl = 1ppbv). This corresponds to a removal time of HCl (via this heterogeneous reaction) of 19 hours (and 3 days for $\gamma = 1.7\times10^{-4}$ at 15 hPa). Thus, we estimate that conversion of HCl to Cl_2 occurs rather quickly inside the volcanic plume, in about 1 to 3 days. This reaction converts inorganic chlorine (HCl and $ClONO_2$) to the free radical form ClO (via photodissociation of Cl_2). Elevated ClO concentrations observed by MLS in the week

following the HT eruption are most likely the result of heterogeneous conversion of HCl to ClO on sulfate aerosols due to a combination of water vapor enhancements and radiative cooling in the stratosphere.

Date of balloon flight	Burst altitude (km)	ECC	CFH	COBALD	POPS	SO_2
20 Jan, 17UTC	28.8	x	x	x		
21 Jan, 19UTC	30.3	x			x	x
21 Jan, 21UTC	20.0	x	x	x		
22 Jan, 18UTC	31.6	x			x	x
22 Jan, 21UTC	31.5	x	x	x		
23 Jan, 00UTC	26.4	x			x	x
23 Jan, 18UTC	30.6	x	x	x		
24 Jan, 15UTC	31.2	x			x	x
24 Jan, 17UTC	31.0	x	x	x		

Table S1. Summary of balloon flights from 20 to 24 January 2022 for the rapid response experiment at Maïdo Observatory.

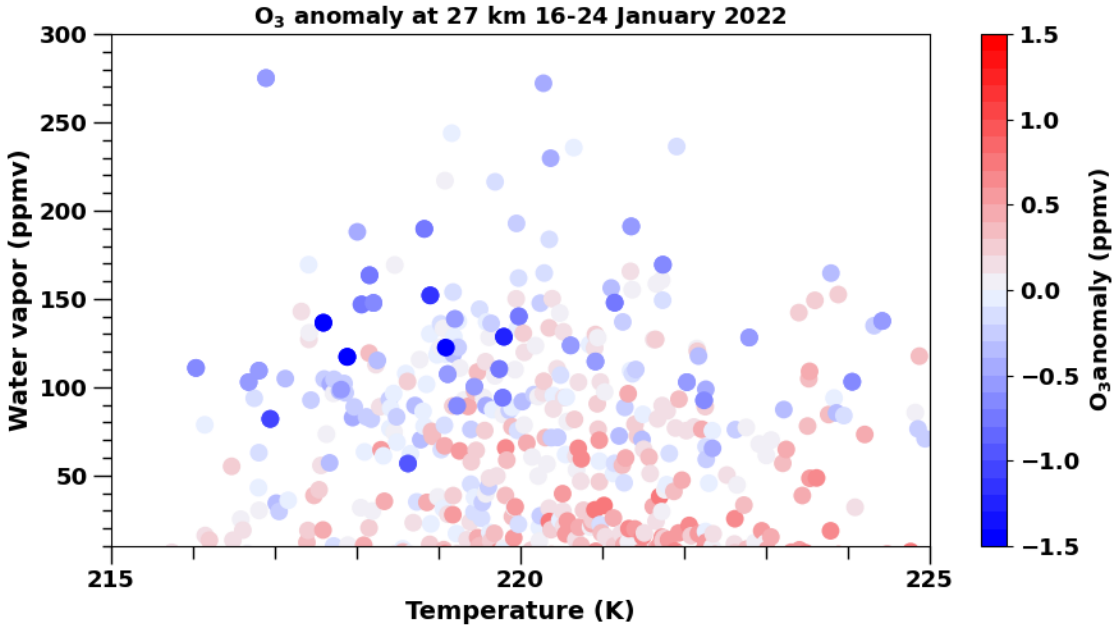

Fig. S1. Scatter plots of ozone anomalies at 27 km versus temperature and water vapor inside the volcanic plume. The ozone anomalies are relative to the January 2005-2021 climatology for MLS data points shown on Figure 2a (i.e., MLS ozone profiles for the period 16-24 January 2022 which are associated with water vapor exceeding 10 ppmv between 10 and 100 hPa).

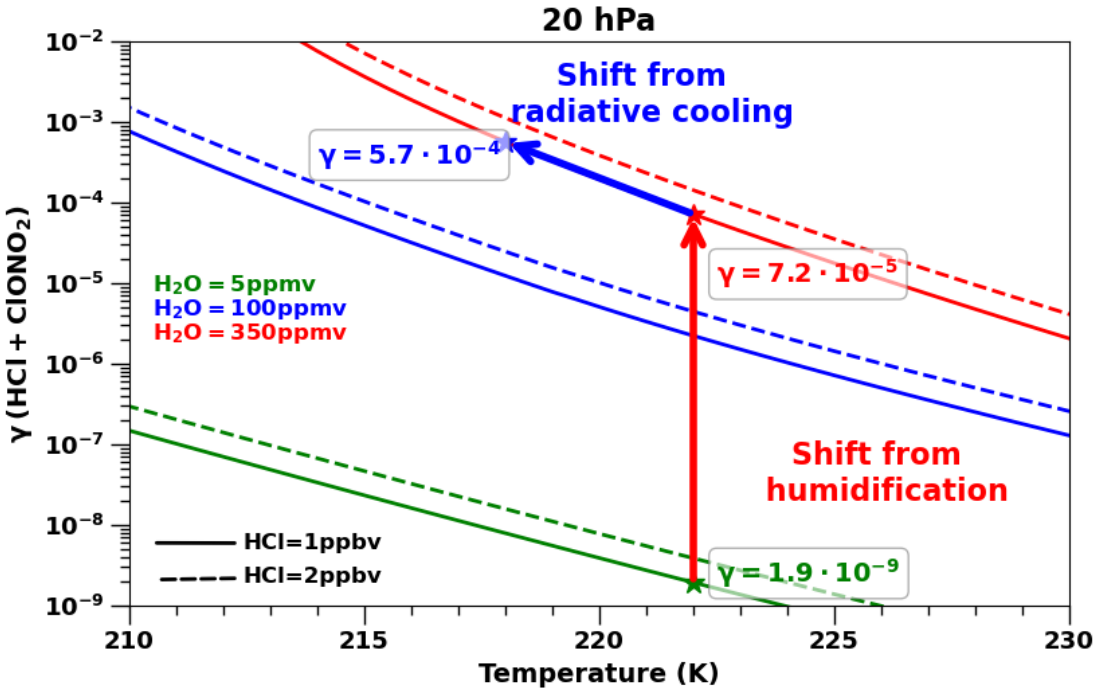

Fig. S2. γ values for HCl+ClONO$_2$ in the stratosphere as a function of temperature between 210 and 230 K at 20 hPa, aerosol radius 0.3 µm, and H$_2$O of 5 ppmv (green), 100 ppmv (blue) and 350 ppmv (red), HCl of 1 ppbv (solid line) and 2 ppbv (dashed line) and 0.5 ppbv of C1ONO$_2$. The red arrow indicates the shift in γ values from humidification from 5 to 350 ppmv and the blue arrow indicates the shift in γ values from a -4 K radiative cooling.

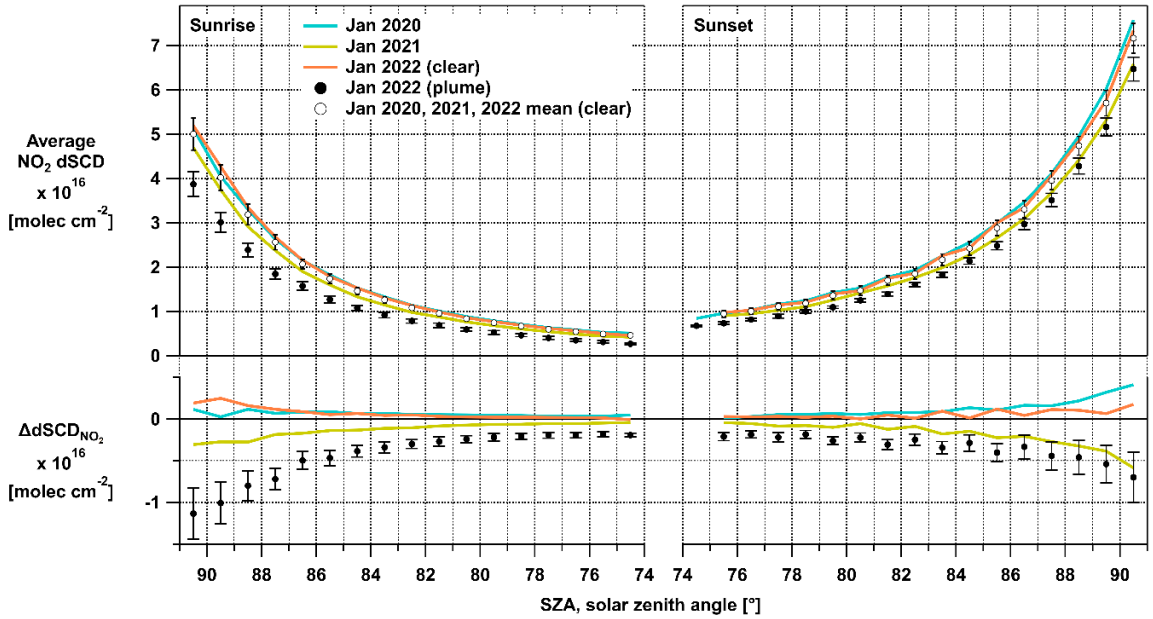

Fig. S3. Stratospheric NO_2 is reduced compared to the clear-sky interannual mean NO_2 during January 2020, 2021, 2022. Zenith-sky DOAS observations reveal reductions in the NO_2 differential slant column density (dSCD) during sunrise (left) and sunset (right) which is attributed to N_2O_5 hydrolysis. The bottom panel shows the difference relative to the clear-sky interannual mean. Aerosols could have increased NO_2 dSCDs for SZA < 90 deg, and thus the NO_2 decrease is an estimated lower limit. Data have been binned by solar zenith angle (SZA). Error bars indicate 95% confidence intervals within each bin (plume) and annual baseline variability (clear); for SZA larger 75 deg each bin contains 17 NO_2 dSCDs (avg. inside plume; range: 11-40 measurements); and 76 NO_2 dSCDs (avg. interannual mean; range: 44-98 measurements).